Journal Pre-proofs

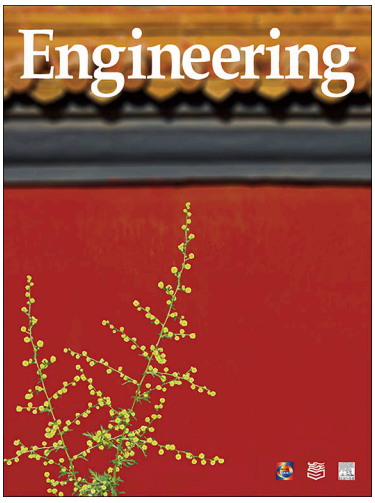

Article

Experimental Exploration of An Ammonia Cracking Power Generation System for Electric Aircraft Propulsion

Chiu Shek Wong, Zaixing Wang, Shuvra Saha, Haoyu Zhao, Yashan Lin, Song Cheng, Jie Mei, Wing Wa Chan, Shu Chuen Ip, Junkui Mao, Ka Wai Eric Cheng, Molly Meng-Jung Li

PII: S2095-8099(26)00120-7
DOI: https://doi.org/10.1016/j.eng.2026.02.021
Reference: ENG 2275

To appear in: *Engineering*

Received Date: 17 June 2025
Revised Date: 7 February 2026
Accepted Date: 11 February 2026

Please cite this article as: C.S. Wong, Z. Wang, S. Saha, H. Zhao, Y. Lin, S. Cheng, J. Mei, W.W. Chan, S.C. Ip, J. Mao, K.W. Eric Cheng, M.M-J. Li, Experimental Exploration of An Ammonia Cracking Power Generation System for Electric Aircraft Propulsion, *Engineering* (2026), doi: https://doi.org/10.1016/j.eng.2026.02.021

This is a PDF of an article that has undergone enhancements after acceptance, such as the addition of a cover page and metadata, and formatting for readability. This version will undergo additional copyediting, typesetting and review before it is published in its final form. As such, this version is no longer the Accepted Manuscript, but it is not yet the definitive Version of Record; we are providing this early version to give early visibility of the article. Please note that Elsevier's sharing policy for the Published Journal Article applies to this version, see: https://www.elsevier.com/about/policies-and-standards/sharing#4-published-journal-article. Please also note that, during the production process, errors may be discovered which could affect the content, and all legal disclaimers that apply to the journal pertain.

© 2026 THE AUTHORS. Published by Elsevier LTD on behalf of Chinese Academy of Engineering and Higher Education Press Limited Company

Journal Pre-proofs

Green Aviation Propulsion—Article

Experimental Exploration of An Ammonia Cracking Power Generation System for Electric Aircraft Propulsion

Chiu Shek Wong[a,#], Zaixing Wang[a,#], Shuvra Saha[a], Haoyu Zhao[a], Yashan Lin[a], Song Cheng[b], Jie Mei[c], Wing Wa Chan[c], Shu Chuen Ip[c], Junkui Mao[d,*], Ka Wai Eric Cheng[c,*], Molly Meng-Jung Li[a,*]

[a] *Department of Applied Physics, The Hong Kong Polytechnic University, Hong Kong 999077, China*

[b] *Department of Mechanical Engineering, The Hong Kong Polytechnic University, Hong Kong 999077, China*

[c] *Department of Electrical and Electronic Engineering, The Hong Kong Polytechnic University, Hong Kong 999077, China*

[d] *College of Energy and Power Engineering, Nanjing University of Aeronautics and Astronautics, Nanjing 210016, China*

[#] These authors contributed equally to this work.
*Corresponding authors.
Email addresses: mjkpe@nuaa.edu.cn (J. Mao), eric-cheng.cheng@conect.polyu.hk (K. W. E. Cheng), molly.li@polyu.edu.hk (M. M.-J. Li)

Abstract

The aviation sector faces growing pressure to reduce carbon emissions, and electric propulsion systems (EPS) based on proton exchange membrane fuel cells (PEMFCs) provide a promising path toward sustainable, zero-carbon aviation. However, challenges related to hydrogen storage and transport have hindered the practical implementation of such systems. Ammonia (NH_3), with high energy density, convenient storage and transport, and carbon neutrality, has emerged as an attractive hydrogen carrier. This study proposes and experimentally validates a compact NH_3 cracking power generation system tailored for EPS through laboratory-scale exploration, engineering-scale validation, and system-level evaluation. The system delivers a maximum power output of 30 kW and comprises a custom-designed multifunctional NH_3 cracking reactor with integrated heat recovery, a temperature swing adsorption (TSA) purification unit, and PEMFC stacks. To meet practical application needs, this study screens and optimizes a commercially available 1% Ru – Ni/Al_2O_3 catalyst, achieving over 99% NH_3 conversion under realistic conditions. The TSA unit reduces NH_3 concentration to below the detection limit, ensuring stable PEMFC performance with a single-stack maximum power output of 5.3 kW. Simulation results further show that the multi-stage thermal management increases the propulsion usable net electrical efficiency to 20.52%, and further raises the overall energy efficiency to 28.33% when the low-grade recovered heat is assumed fully usable. The optimized system achieves a gravimetric energy density of 692.7 $W \cdot h \cdot kg^{-1}$ and a hydrogen storage capacity of 6.7 wt% when equipped with five NH_3 tanks, each containing 22.7 kg of NH_3. This work demonstrates an NH_3-powered PEMFC EPS for aviation, offering both experimental validation and theoretical guidance for NH_3-fueled propulsion technologies. The study provides system-level insights into design, integration, and performance optimization, supporting the future development of electrified aviation and related zero-carbon distributed energy systems.

Keywords: Electric propulsion system; Ammonia cracking; Catalyst optimization; Thermal management; Energy efficiency

1. Introduction

As the global climate change problem intensifies, air transportation faces increasing pressure to reduce carbon emissions [1–3]. Traditional aircraft propulsion systems mainly rely on fossil-fueled heat engines, such as turbojet and piston engines, which emit large amounts of carbon dioxide (CO_2) and pose serious environmental risks [4,5]. According to the International Energy Agency (IEA), aviation CO_2 emissions grew faster than those of rail, road, or shipping between 2000 and 2019, peaking at over 1.03 Gt in 2019. Following the coronavirus disease 2019 (COVID-19) pandemic, this figure fell below 600 Mt in 2020, rebounded to 950 Mt (2.5% of global emissions) by 2023, and is expected to surpass the 2019 peak by 2025 [6]. The development of sustainable, low-emission propulsion systems is now a central concern in aerospace engineering.

Electric propulsion systems (EPS) have recently attracted widespread attention in aviation research, characterized by high energy efficiency, low noise, and zero emissions [7,8]. Electric propulsion plays a key role in aviation decarbonization and energy transition, regarded as a critical enabler of future green aviation [9]. EPS has achieved initial deployment in commuter aircraft, electric vertical take-off and landing (eVTOL) aircraft, and fixed-wing platforms [10–12]. However, the predominant power source of EPS is the lithium-ion battery with limited energy density (100 – 350 $W \cdot h \cdot kg^{-1}$), which is generally suitable for short-range flights and incapable of meeting long-endurance operations [13–15]. As electric aviation evolves to broader commercial applications, the demand for higher energy density and extended flight range has become urgent.

Proton exchange membrane fuel cell (PEMFC) generates electricity through the electrochemical reaction between hydrogen (H_2) and oxygen (O_2), with notable advantages such as being pollution-free, lightweight, and having a high energy density [16–18]. PEMFC has matured commercially in automotive propulsion systems, as exemplified by Toyota's second-generation Mirai, whose fuel cell stack achieves volumetric and gravimetric power densities of 5.4 $kW \cdot L^{-1}$ and 2.46 $kW \cdot kg^{-1}$, respectively [19]. To address the limitations of conventional battery systems, PEMFC has emerged as a promising alternative

energy source for integration into EPS. Depcik et al. [20] compared lithium-ion batteries, H_2-fueled combustion engines, and PEM [boilerplate] erior integrability, delivering power directly without complex mechanical systems, and meets the specific power requirements of EPS.

Although PEMFC has demonstrated viability in automotive and related transport sectors, persistent technical barriers to H_2 storage and transportation issues hinder the broader adoption in aviation [21,22]. Gaseous H_2 requires high-pressure storage (350 – 700 bar), while liquid H_2 demands cryogenic temperatures (−253 °C), which creates complexity and stringent safety requirements for aerospace applications [23]. In contrast, ammonia (NH_3) has gained growing interest as a chemical H_2 carrier, owing to its high H_2 content (17.7 wt%), carbon-free composition, and relatively mild liquefaction conditions (9 bar at 20 °C) [24–26]. Most of all, NH_3 is already mass-produced via the well-established Haber – Bosch process, and benefits from an existing supply chain [27].

Furthermore, NH_3 can undergo a cracking reaction at medium-to-high temperatures (typically 450 – 700 °C) over suitable catalysts, yielding H_2 and nitrogen (N_2) without carbon emissions [28]. Most aviation-oriented studies have explored combining NH_3 cracking with combustion-based propulsion systems to drive conventional thermomechanical cycles through simulation. For example, Wang et al. [29] proposed a precooled engine cycle concept for supersonic aircraft that utilizes NH_3 cracking, leveraging the endothermic reaction to control engine temperature and enhance flame speed. Boretti [30] introduced a hybrid eVTOL aircraft that incorporates an onboard NH_3 cracker to generate H_2 for jet ignition, thereby mitigating slow combustion. However, combining NH_3 cracking with combustion propulsion poses many challenges, such as high NO_x emissions and complex combustion control, which affect the pace and pathway of deployment for next generation clean propulsion systems [31,32].

An alternative approach is to integrate NH_3 cracking with PEMFC, enabling a complete "NH_3 – H_2-electricity" power generation pathway, and providing a stable and environmentally friendly energy source [33]. However, current research on such NH_3-based power systems is confined to low-power experimental prototypes or simulation-based analyses, with most efforts toward automotive, maritime transportation, and stationary power applications.

For the simulation studies, integrated NH_3-based power systems have been investigated and evaluated through system conceptual design. Xu et al. [34] proposed an NH_3 cracking hybrid power system integrating PEMFC with internal combustion engines (ICE) for automotive applications, employing simulation to evaluate thermodynamic, economic, and environmental performance. Di Micco et al. [35] designed and modeled an NH_3-based propulsion system for shipping, including PEMFC, NH_3 cracker, pressure swing adsorption (PSA), and catalytic burner. Lin et al. [36] conducted a comprehensive simulation analysis of an indirect NH_3-PEMFC (IA-PEMFC) system for a power generation station. More recently, Massaro et al. [37] proposed a conceptual design integrating an NH_3 cracker with the PEMFC system for regional aircraft, achieving a promising gravimetric H_2 storage index of 9.1%, demonstrating the feasibility and competitiveness of NH_3-based storage for aviation.

Nevertheless, system-level experimental studies are still scarce, and existing implementations are limited to small-scale, low-power platforms. For example, Zhang et al. [38] employed magnetic induction heating to rapidly start NH_3 cracking in a miniature PEMFC-powered car, with a fuel flow rate of 50 $mL \cdot min^{-1}$. Hunter et al. [39] established an experimental platform comprising an NH_3 cracker, gas purification column, and PEMFC, producing an output power of about 40 W. Cha et al. [40] constructed a power pack consisting of an NH_3 cracker, an adsorbent tower, and a 1 kW-class PEMFC to treat NH_3 at 9 $L \cdot min^{-1}$, and demonstrated stable operation over two hours. The system is successfully applied as a tethered ground power source, supplying continuous power to a UAV through the cable, enabling extended flights of more than four hours. In addition, in our previous study, we developed and validated a 300 W NH_3-powered PEMFC electric golf cart system, highlighting the potential of NH_3 as a viable, carbon-free H_2 carrier for automotive applications [41].

While these pioneering studies have demonstrated the feasibility of NH_3-PEMFC integration in small-scale scenarios, most remain centered on individual components or simplified subsystems, with limited exploration of fully integrated platforms suitable for EPS. To bridge this critical gap, it is essential to experimentally validate a high-power scale, fully integrated ammonia-to-electricity conversion system to provide foundational insights for EPS-related applications.

This work proposes an integrated NH_3 cracking fuel cell power system incorporating an NH_3 cracker, a temperature swing adsorption (TSA) gas purification unit, and a PEMFC stack. A custom-developed energy management system (EMS) with an embedded Internet of Things (IoT) network enables real-time monitoring and precise control of critical parameters, including reactor temperature, gas flow rate, residue ammonia concentration, system pressure, and fuel cell output power. In addition, a system-level simulation platform is designed in parallel with the experimental setup, allowing for performance optimization and evaluation based on experimental data. Fig. 1 demonstrates a conceptual diagram of the integrated system deployment in an aircraft, providing an overall overview of the main components and layout for aviation applications. This study marks a significant advancement in experimental, system-level demonstrations of NH_3-based power systems, laying the groundwork for scalable carbon-free propulsion solutions with potential integration into next-generation electric aircraft.

Journal Pre-proofs

Journal Pre-proofs

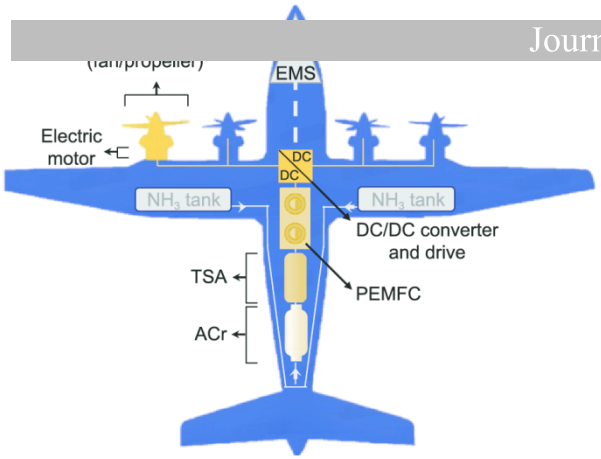

Fig. 1 Schematic diagram of the integrated NH_3-fueled electric propulsion system for aviation applications. DC: direct current; ACr: NH_3 cracker.

2. Experimental system description

Fig. 2 presents the physical layout and schematic diagram of the NH_3 cracking power generation experimental system developed in this study. A detailed system flowchart, including all test components and connections, is provided in Fig. S1 in Appendix A. Designed with compactness and aviation applicability in mind, the system integrates NH_3 cracker (ACr), TSA, PEMFC stack, buffer tank (BT), and balance of plant (BOP) components, including flow meters, pressure regulators, solenoid valves, and various sensors for real-time monitoring and control (Fig. S1). The experimental procedure comprises three major steps: catalyst activation, power generation, and TSA regeneration, and details of the experimental procedures are provided in Section S1.1 in Appendix A.

The integrated system consists of five subsystems, as shown in Fig. S1: Fuel Supply Subsystem (FSS), Catalytic Cracking Subsystem (CCS), Adsorption & Desorption Subsystem (ADS), Power Generation Subsystem (PGS), and Exhaust Treatment Subsystem (ETS). The basic operating principle of this system is as follows:

After complete reduction of the cracking catalyst, liquid ammonia stored at around 25 °C and 10 bar is first vaporized at 3 bar and then fed into ACr at the specified flow rate. To minimize the volume and maximize thermal efficiency, a custom-designed multifunctional reactor (see Section S1.5 in Appendix A) is developed, which integrates feed gas preheating, catalytic reaction, and internal heat recovery within a single compact unit. A liquid coolant circulates to absorb heat from the product gas and simultaneously preheat the NH_3 feed via internal heat exchange. Under the catalytic action of 1 wt% Ru–Ni/Al_2O_3, NH_3 is decomposed at 650 – 700 °C, yielding an H_2/N_2 mixture gas with trace residual NH_3. The mixture is cooled to near room temperature by a cooler (CLr) to match the operating conditions (25 °C, 1 bar) of the TSA unit. Within the TSA, 13X molecular sieves adsorb the residual NH_3, reducing its concentration below the detection limit of the mass spectrometer to meet the PEMFC feed gas requirements.

The purified H_2/N_2 gas is subsequently supplied to the PEMFC stacks for power generation. The fuel cell subsystem comprises six PEMFC units rated at 5 kW each, delivering a maximum output power of 30 kW. BT is installed upstream of the stack to mitigate the adverse effects of H_2 flow fluctuations and ensure stable operation. The system output power is regulated by adjusting the voltage of the electronic load to meet varying power demands.

Journal Pre-proofs

Journal Pre-proofs

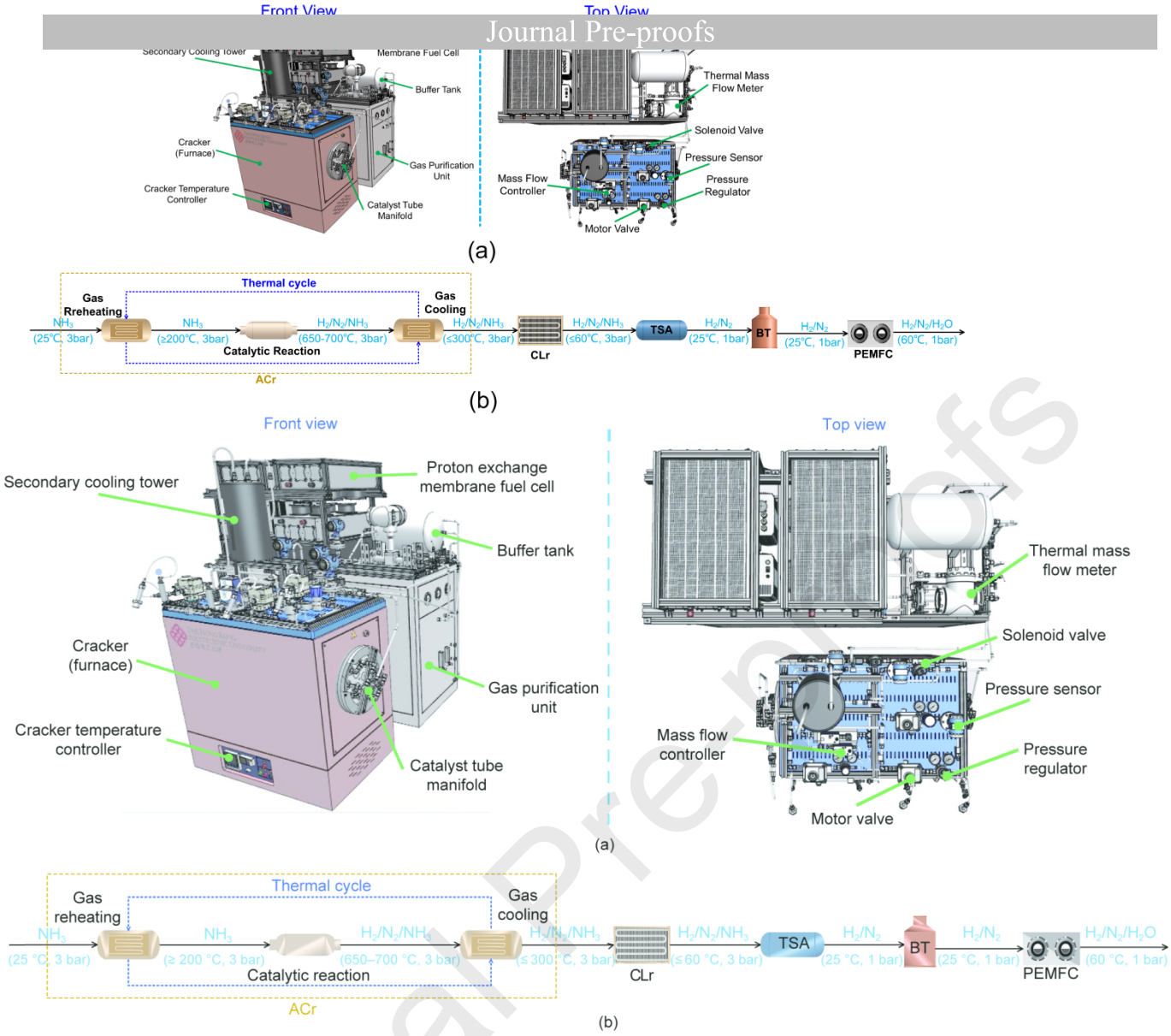

Fig. 2 NH_3 cracking power generation experimental system: (a) three-dimensional (3D) schematic view with dimensions of 200 cm × 180 cm × 170 cm; (b) simplified process flow diagram highlighting the representative operating parameters. BT: buffer tank.

3. Research method

3.1 Catalyst synthesis

In this study, we aim to develop a practical and scalable catalyst suitable for engineering applications by utilizing commercially available catalysts. A series of Ru-based catalysts is synthesized and evaluated for the NH_3 cracking reaction. To ensure engineering applicability, the catalyst candidates are prepared to employ industrially accessible materials (Al_2O_3, Fe_3O_4, CaO/Al_2O_3, and Ni/Al_2O_3), all impregnated with 1 wt% Ru. Among them, Ru – Ni/Al_2O_3 exhibits the highest activity. To further optimize performance, Ru loadings of 0.5%, 1.0%, and 2.0% are tested on the Ni/Al_2O_3 support. The optimized formulation is scaled and packed into a 1-meter long, 1-inch outer diameter stainless-steel tubular reactor, with a total catalyst bed volume of 340 mL. Sections S1.2 – S1.4 in Appendix A provide detailed synthesis procedures and material characterizations.

3.2 Gas purification

The NH_3 cracking reaction is endothermic and limited by thermodynamic equilibrium, resulting in a residual NH_3 concentration of 800 – 1000 parts per million (ppm) in the product gas, which should be removed to avoid potential damage to downstream PEMFC stacks. This study employs a compact TSA unit consisting of two parallel adsorption columns, each filled with 32 L of 13X molecular sieve, as shown in Fig. S7 in Appendix A.

3.3 Power generation

PEMFC serves as the core of the power generation subsystem, with six stacks connected in parallel. Fig. S8 in Appendix A sh[illegible]gnal pathways. Each PEMFC stack contains 120 cells with an activation area of 165 cm^2. The stacks employ H_2 and air as reactants, with an air-cooled open-cathode design and a fan for heat dissipation. The utilization ratios of hydrogen at the anode and oxygen at the cathode in the PEMFC stack are 0.78 and 0.50, respectively, corresponding to stoichiometric ratios of 1.28 and 2, as expressed in Appendix A Eqs. (S10) and (S11).

To evaluate the performance of PEMFC stacks under practical operating conditions, tests are conducted under two different gas feeds: pure H_2 (99.99%) and H_2/N_2 mix gas (75/25) to simulate the output composition of NH_3 cracking. These tests aim to assess the effect of N_2 dilution on the electrical output of the PEMFC stacks.

3.4 Process simulation

Based on the experimental results, a simulation method is adopted to evaluate the maximum NH_3 inlet flow rate, H_2 production, power output, and overall system performance. A co-simulation strategy combining Aspen Plus and MATLAB/Simulink is employed in this work, which was previously developed in our earlier work [42]. The detailed modeling procedures and parameter settings are provided in Appendix A Section S2.

In this study, two system efficiency calculation methods (Methods 1&2) are adopted in this work, and the system performance is evaluated from two perspectives, namely the electrical efficiency and the overall energy efficiency.

Method 1 uses the net electricity output as the numerator, where the auxiliary consumption is subtracted from the PEMFC stack output, and the lower heating value (LHV) of the fuel input normalizes the result:

Eqs. (1) and (2) represent the electrical efficiency for Systems I and II, respectively.

$$\eta_{\text{System I}} = \frac{W_{\text{PEMFC}} - Q_{\text{Cracker}} - Q_{\text{Preheat}}}{n_{\text{NH}_3} \cdot \text{LHV}_{\text{NH}_3}} \quad (1)$$

$$\eta_{\text{System II}} = \frac{W_{\text{PEMFC}} - Q^*_{\text{Cracker}}}{n_{\text{NH}_3} \cdot \text{LHV}_{\text{NH}_3}} \quad (2)$$

Eq. (3) defines the overall energy efficiency for System III, which combines the electrical output and usable recovered heat.

$$\eta_{\text{System III}} = \frac{W_{\text{PEMFC}} - Q^*_{\text{Cracker}} + \varepsilon \cdot Q_{\text{Recovery}}}{n_{\text{NH}_3} \cdot \text{LHV}_{\text{NH}_3}} \quad (3)$$

where W_{PEMFC} denotes the output power of the PEMFC stack; Q_{Preheat} is the supply heat for preheating the fuel; Q^*_{Cracker} is the remaining supply heat of the cracker; Q_{Recovery} is the heat recovery; n_{NH_3} and $\text{LHV}_{\text{NH}_3}$are the inlet flow rate and low heating value (18.6 $MJ \cdot kg^{-1}$) of NH_3; ε ranges from 0 to 1 and represents the fraction of recovered heat that is actually usable:

(1) $\varepsilon = 0$ corresponds to applications without a thermal load, where only electrical output is considered, such as UAV propulsion;

(2) $0 < \varepsilon < 1$ represents practical cases where recovered heat is partially utilized;

(3) $\varepsilon = 1$ denotes the ideal upper bound, in which the recovered heat is fully absorbed and delivered to an effective thermal load.

Method 2 is defined as a gross output-based efficiency evaluation under the experimental conditions, where the cracker and preheater are powered by external supplies rather than by the PEMFC stack output. The detailed expressions are provided in Appendix A as Eqs. S19 – S21.

It should be noted that, in the present experimental setup, the power consumption of other auxiliary components, such as DC/DC converters, electromagnetic valves, and other BOP components, is negligible compared with the heat supplied for fuel preheating and ammonia cracking. Therefore, these minor losses are not included in the above efficiency formulations.

4. Results and discussion

4.1 Catalyst characterization

Current state-of-the-art lab-developed NH_3 decomposition catalysts often require complex or delicate synthesis procedures, which limit their scalability. To avoid the costly and time-consuming transition from lab scale to practical applications, this study focuses on commercially available materials that require only minor modifications. Through this approach, a scalable, suitable catalyst for engineering applications has been successfully identified. The catalyst evaluation is divided into three stages: laboratory-scale screening, engineering-scale validation, and simulation-based performance prediction, as illustrated in Figs. 3(a) – (d).

Figs. 3(a) and (b) present the NH_3 conversion of Ru-doped catalysts under laboratory conditions. In these tests, 0.1 g of each catalyst is used with a fixed weight hourly space velocity (WHSV) of 30 000 $mL_{NH3} \cdot h^{-1} \cdot g_{cat}^{-1}$, and reaction temperatures range from 450 to 650 °C. As shown in Fig. 3(a), the performance of different catalysts varies widely. Among the four Ru-modified commercial supports (Al_2O_3, Fe_3O_4, CaO/Al_2O_3, and Ni/Al_2O_3), 1% Ru-Ni/Al_2O_3 catalyst shows the highest NH_3 conversion across the temperature range, while 1% Ru-Fe_3O_4 and 1% Ru-CaO/Al_2O_3 perform the worst. For example, at 600 °C, the NH_3 conversion of 1% Ru-Ni/Al_2O_3 catalyst reaches 97.82%, while 1% Ru-CaO/Al_2O_3 has only 39.06%. This comparison confirms that the Ru-modified Ni/Al_2O_3 catalyst exhibits higher catalytic activity for NH_3 cracking.

Building on these findings, Fig. 3(b) compares different Ru loadings (0.5%, 1.0%, and 2.0%) on the Ni/Al_2O_3 support. The resu [boilerplate: Journal Pre-proofs] °C. In contrast, a higher Ru loading of 2% leads to reduced performance, dropping to 82.8% at the same temperature. This result suggests 1 wt% Ru is closer to the optimal dispersion for the catalyst formulation and preparation method employed in this work [43,44]. The Coupled Plasma-Optical Emission Spectroscopy (ICP-OES) analysis in Appendix A Table S1 indicates that approximately 0.7 wt% of Ru is actually deposited on the Ni/Al_2O_3 support surface. These results confirm that 1% Ru – Ni/Al_2O_3 is the optimal catalyst among the selected commercial materials and is therefore chosen for subsequent engineering-scale evaluation. Fig. 3(c) shows the NH_3 conversion of the optimized 1% Ru – Ni/Al_2O_3 catalyst in a scaled-up reactor. Figs. S4 and S5 in Appendix A details specifications of the scaled-up reactor, consisting of a 1-meter-long stainless-steel tube with a 1-inch outer diameter, packed with 340 mL of catalyst. Tests with NH_3 flow rates range from 5 to 9 $L \cdot min^{-1}$, corresponding to gas hourly space velocities (GHSV) of 882 to 1588 h^{-1}, at reaction temperatures between 500 and 700 °C. The catalyst performs excellently, exceeding 99% NH_3 conversion above 650 °C, even at the highest flow rates.

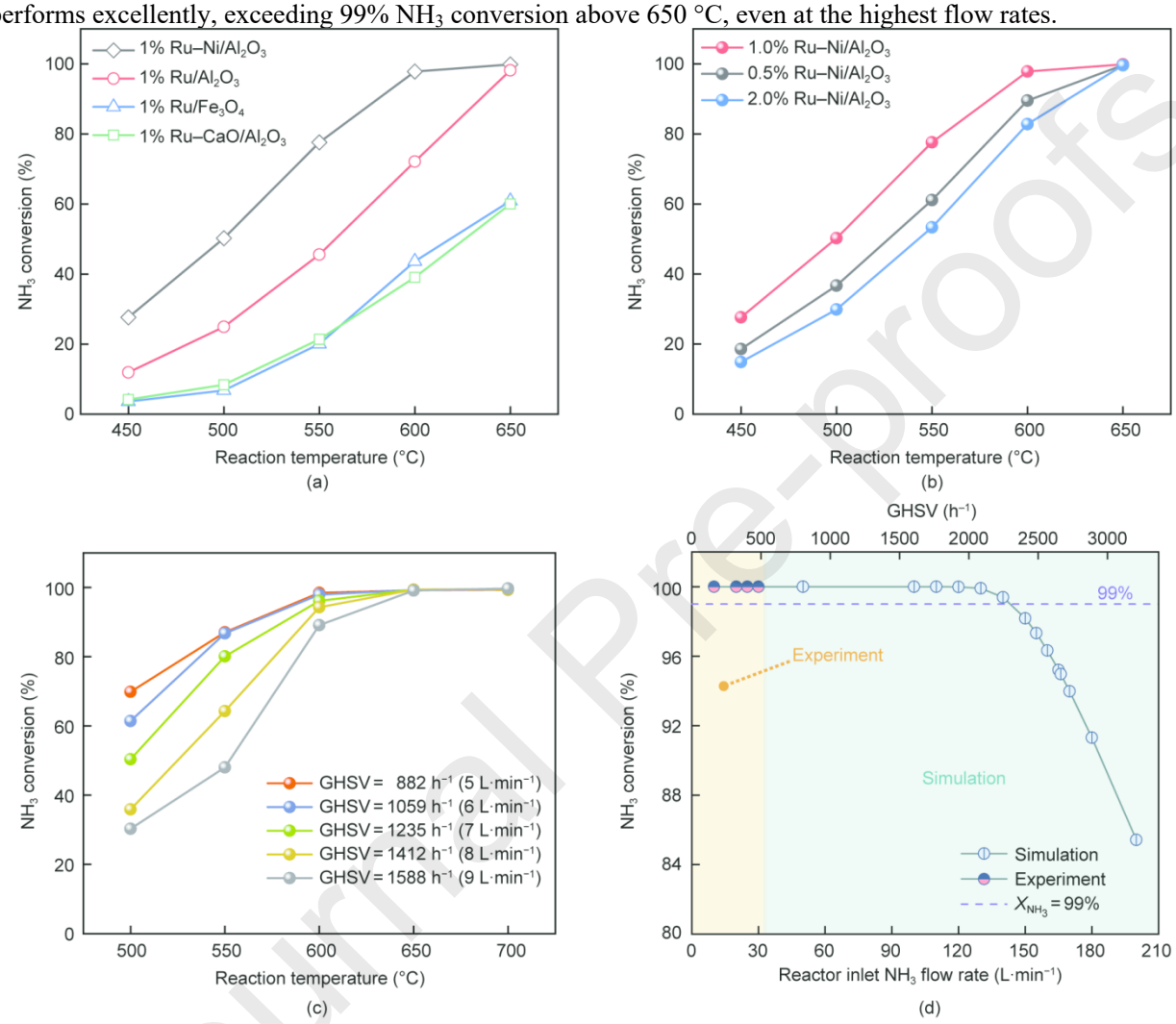

Fig. 3 Performance evaluation of NH_3 cracking catalysts under varying reaction conditions: (a) Comparison of different commercial catalysts with 1 wt% Ru loading at WHSV = 30 000 $mL_{NH3} \cdot h^{-1} \cdot g_{cat}^{-1}$; (b) optimization of Ru loading on Ni/Al_2O_3 supports (0.5%, 1.0%, and 2.0% Ru); (c) NH_3 conversion in a scaled-up tubular cracker under different inlet flow rates (5 – 9 $L \cdot min^{-1}$) (GHSV: gas hourly space velocities, volumetric flow rate of NH_3/volume of catalyst); (d) simulation and experimental analysis of NH_3 conversion for determining the maximum allowable NH_3 inlet flow rate in eleven parallel tube cracker.

Furthermore, the long-term stability of the optimized 1% Ru – Ni/Al_2O_3 catalyst is evaluated under continuous operation for a cumulative 60 hours at 650 °C, as shown in Appendix A Fig. S6. The test is conducted using a 1-meter stainless steel tubular reactor packed with 340 mL of catalyst, with a constant NH_3 flow rate of 9 $L \cdot min^{-1}$. Due to the high gas throughput, the system is operated in daily cycles of 7.5 to 9.0 hours, with the reactor restarted each day. As shown in the figure, the catalyst maintained excellent stability throughout the entire period, with NH_3 conversion consistently above 99.6% and no observable signs of deactivation, confirming its suitability for extended ammonia decomposition.

Due to strict restrictions on NH_3 storage and handling in Hong Kong [45], the maximum allowable NH_3 flow rate for experimental testing is limited to 30 $L \cdot min^{-1}$. Therefore, engineering-level experimental tests are performed with eleven parallel stainless steel reaction tubes up to 30 $L \cdot min^{-1}$. To address higher flow rates beyond the experimental constraints, a simulation model is developed to predict catalytic performance. The simulation is implemented using the kinetic parameters of the optimized 1% Ru – Ni/Al_2O_3 catalyst, derived from laboratory experiments and expressed in Eq. S6, thereby ensuring consistency between the experimental data and model predictions. As shown in Fig. 3(d), the NH_3 cracker maintains a

conversion above 99% when the inlet flow rate is below 125 L·min^{-1}. Even at higher flow rates, such as 180 L·min^{-1}, the systJournal Pre-proofs the performance stability and practical engineering constraints, a nominal inlet flow rate of 125 L·min^{-1} is selected as the design target for subsequent system integration and performance evaluation.

4.2 TSA performance evaluation

To ensure that the H_2 meets PEMFC requirements, a TSA unit is used for NH_3 purification. Figs. 4(a) and (b) display the structural diagram and breakthrough behavior of the TSA experimental setup with a 13X molecular sieve. The test is designed to simulate practical conditions and evaluate the maximum continuous operation time of the TSA unit.

The actual product gas from NH_3 cracking consists of an H_2/N_2 mixture with a total flow rate of around 250 L·min^{-1} and a residual NH_3 concentration of about 800 – 1000 ppm. As shown in Fig. 4(a), the test system continuously feeds a gas mixture of 300 L·min^{-1} of air and 0.3 L·min^{-1} of NH_3 into a two-column TSA unit, with adsorption conducted at room temperature. The NH_3 concentration at the inlet is approximately 1000 ppm, as confirmed by an ammonia sensor and a mass spectrometer.

Following the TSA treatment, Fig. 4(b) shows that the outlet NH_3 concentration remains below the detection limit of the mass spectrometer for the first 600 min, indicating stable and effective adsorption performance. Beyond this duration, a sharp increase is observed, with the concentration exceeding 1000 ppm within 100 min, signaling the breakthrough and saturation of the adsorbent. This breakthrough curve confirms the strong adsorption capacity of 13X molecular sieves for NH_3 and demonstrates the capability of TSA for long-duration continuous operation. The dual-column design enables alternating adsorption and desorption cycles, supporting uninterrupted purification and stable downstream H_2 utilization.

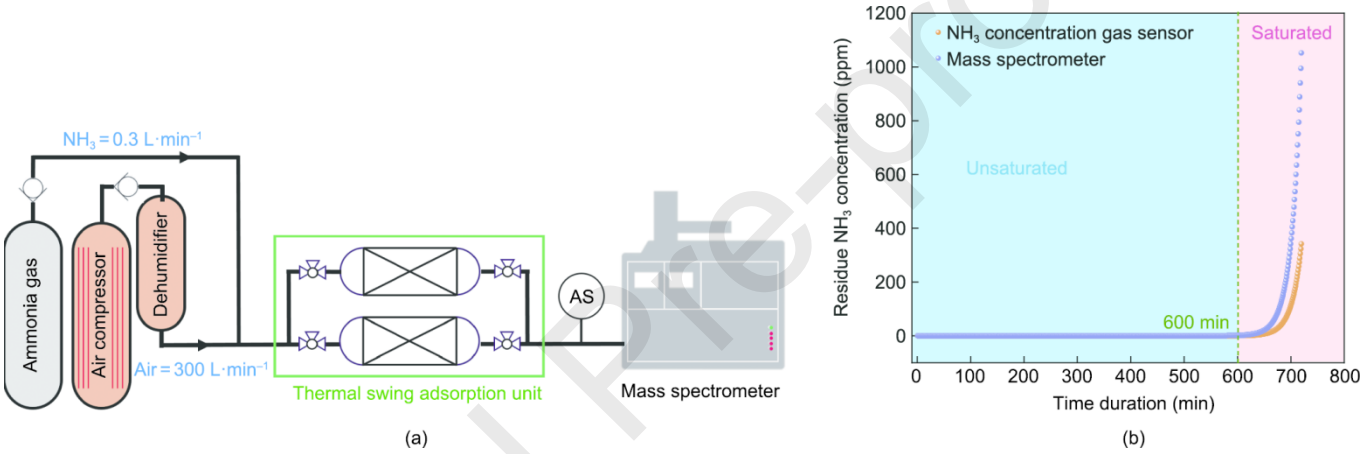

Fig. 4 Experimental setup and breakthrough behavior of the TSA unit. (a) schematic of the two column TSA experimental setup; (b) breakthrough curve of outlet NH_3 concentration during TSA adsorption.

4.3 PEMFC testing and simulation

Figs. 5(a) and (b) present the experimental and simulation performance of PEMFC under varying inlet gas compositions and pressures. The voltage – current – power (V-I-P) characteristics are shown for three conditions: (i) pure H_2 at 0.5 bar, (ii) 75% H_2/25% N_2 at 0.5 bar, and (iii) 75% H_2/25%N_2 at 0.3 bar. The simulation parameters are calibrated based on the experimental setup and PEMFC configurations.

As displayed in Fig. 5(a), as the load current increases from 0 to 55 A, the stack voltage decreases under all operating conditions. The voltage drops from 116.9 to 90.8 V in condition (i), from 116.5 to 86.6 V in condition (ii), and more significantly from 116.3 V to 80.6 V in condition (iii). Furthermore, lowering the operating pressure from 0.5 to 0.3 bar further aggravates the voltage loss due to limited reactant availability and increased mass transport resistance [46]. In Fig. 5(b), the output power increases with current and reaches a peak value of approximately 5 kW under optimal conditions. Despite dilution from the H_2/N_2 mixture, the PEMFC exhibits stable and reliable performance, with no signs of irreversible degradation under the present operating conditions, consistent with findings reported in the literature (see Section S1.7 in Appendix A) [47]. On the other hand, the strong consistency between the experimental data and the simulation results further validates the accuracy and robustness of the PEMFC electrochemical model.

In addition, Fig. S9 in Appendix A presents a constant current stability test of the PEMFC stack under a diluted anode feed of 75% H_2/25% N_2. During 80 min of continuous operation at 20 A, the stack delivered stable power output with an average of 1983 W and no discernible power decay. These results demonstrate stable PEMFC operation with a 75% H_2/25% N_2 mixture as the anode feed under the tested conditions.

Journal Pre-proofs

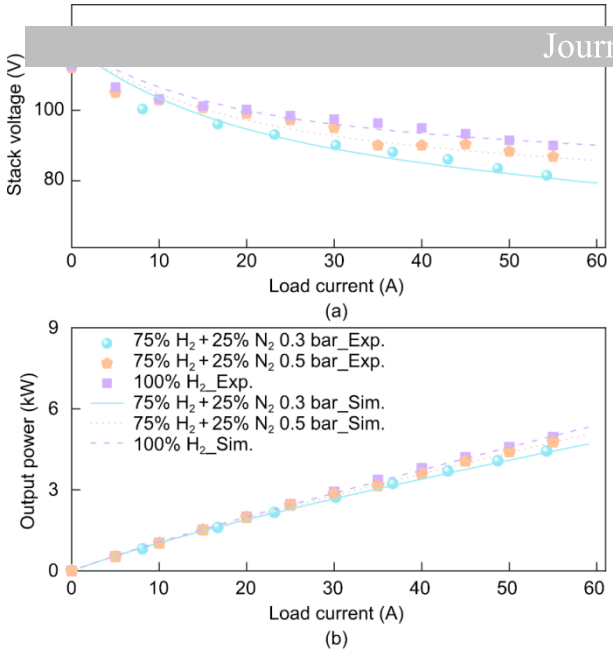

Fig. 5 Voltage – current – power (V-I-P) characteristic curves of PEMFC under varying inlet gas compositions and pressures (0.3 to 0.5 bar are gauge pressures). (a) polarization curve (V–I); (b) power curve (P–I). Exp.: experiment; Sim.: simulation.

4.4 System experimental performance

This section presents the system experimental results, covering the entire NH_3-to-power process from the NH_3 feed to cracking reaction, TSA purification, and PEMFC power generation. Figs. 6(a) and (b) shows the NH_3 inlet flow rate, corresponding H_2 production, and the output power of the PEMFC stack across load currents ranging from 5 to 30 A. In addition, a Supporting Video of the real-time experimental operation is provided in Appendix A. Constrained by regulatory and safety restrictions on NH_3 usage, the maximum allowable NH_3 flow rate is still limited to below 30 $L \cdot min^{-1}$, and only one PEMFC stack is tested.

As shown in Fig. 6(a), the NH_3 feed rate increases from 4.0 to 23.6 $L \cdot min^{-1}$, while the H_2 production increases from 6.0 to 35.4 $L \cdot min^{-1}$. The H_2/NH_3 flow ratio is close to 1.5, suggesting that the NH_3 cracking reaction approaches thermodynamic equilibrium, yielding a product composition close to the theoretical 75% H_2/25% N_2. Fig. 6(b) illustrates that the PEMFC stack maintains a stable voltage profile with increasing current and delivers a peak output power of about 2.9 kW. This performance matches the V-I-P characteristics obtained with a mixture of H_2/N_2 conditions (75%/25%, 0.3 bar), as shown in Fig. 5, confirming the good performance of the NH_3 cracking and purification system under real operating conditions. Furthermore, a representative data point at 30 A load current is highlighted. At this point, the NH_3 feed rate is 23.6 $L \cdot min^{-1}$, the corresponding H_2 flow rate is 35.4 $L \cdot min^{-1}$, and the reactor temperature reaches 689.3 °C, which is monitored by the inserted thermocouple described in Appendix A Fig. S4. The residual NH_3 concentration at the PEMFC inlet is measured at only 0.87 ppm, and the fuel cell delivers a voltage of 97.4 V and a power output of 2.9 kW.

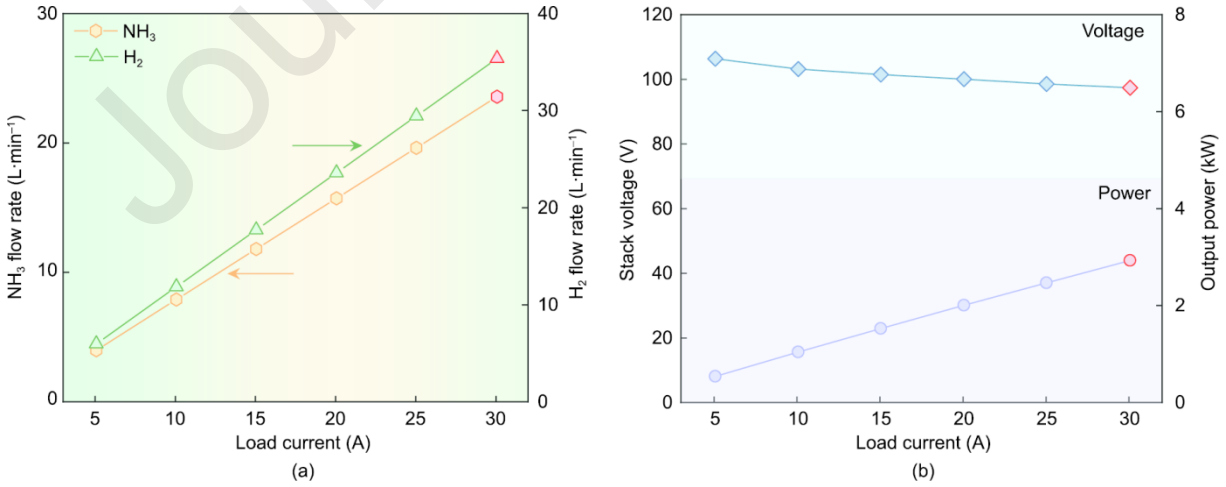

Fig. 6 V-I-P characteristics of PEMFC under the integrated system operation using actual NH_3 cracking gas. (a) NH_3 inlet flow rate and H_2 production rate versus load current; (b) stack voltage and output power versus load current

These experimental results demonstrate that the developed integrated system can operate under realistic dynamic loads and validate the potential for aviation-oriented NH_3-fueled electric propulsion applications.

Journal Pre-proofs

To evaluate the performance of the NH_3 power generation system under realistic operating conditions, a simulation study is performed based on the verified maximum NH_3 inlet flow rate of 125 $L \cdot min^{-1}$, corresponding to an output power of about 12.8 kW. The simulation variables, including operating temperature and component parameters, are aligned with experimental data. Three simplified configurations are designed to estimate different thermal utilization strategies in the integrated system, as demonstrated in Fig. 7. The main difference lies in how each system manages and utilizes thermal energy.

System I is a conventional design that employs an electric preheater (PH) to preheat NH_3. System II corresponds to the current experimental setup, which uses a gas – gas heat exchanger (HEX) to recover thermal energy from the cracker. It is important to note that System II simplifies simulation modeling compared to the actual experimental system. While the experimental system utilizes a multifunctional NH_3 cracking reactor that integrates functions like gas preheating (PH) and cooling (CL), these subcomponents are consolidated into a single HEX in the model. This simplification preserves all core functionalities, keeping the energy balance and operating conditions consistent, and the accuracy of the simulation results is not affected. System III builds upon System II by incorporating an additional heat recovery mechanism from the CL to generate usable hot water.

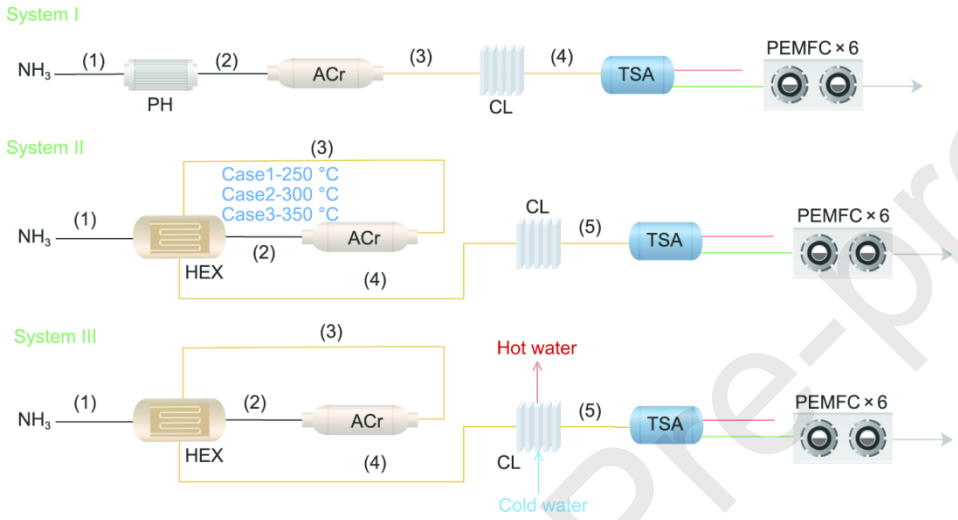

Fig. 7 Structural schematics of three integrated systems with different heat exchange strategies. PH: preheater; HEX: heat exchanger; CL: cooling.

In this simulation study, the reaction temperature is set at 700 °C, the preheating temperature at 300 °C, and the cooling outlet at 60 °C. Considering that, in real operations, the hot-side outlet temperature of the heat exchanger may vary and influence overall system performance, additional cases are investigated in System II with HEX outlet temperatures set at 250, 300, and 350 °C. Fig. 8 compares the system energy efficiency and heat duty among the three systems, while Table 1 provides detailed simulation results corresponding to each configuration.

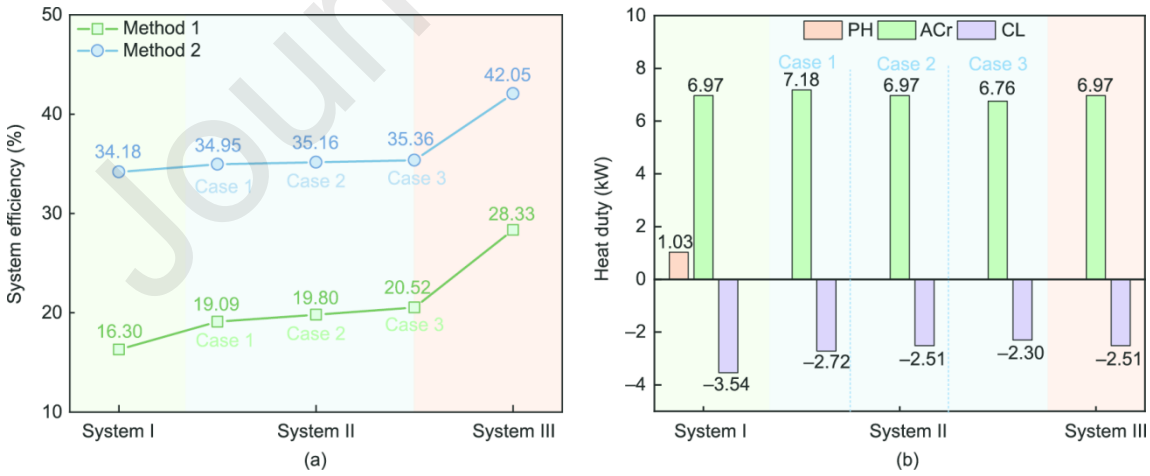

Fig. 8 Comparison of the (a) energy efficiency and (b) component heat duties for the three systems.

System I, which lacks any heat recovery method and relies entirely on external electric heating, has the lowest system efficiency (Method 1) at 16.30%. In contrast, System II achieves higher efficiencies of 19.09%, 19.80%, and 20.52% at HEX outlet temperatures of 250, 300, and 350 °C, respectively. This improvement results from utilizing waste heat from the cracker outlet to preheat the NH_3 feed, thereby reducing external energy demand. Additionally, as the preheating temperature

increases, the heat duty required by the cracker decreases from 7.18 to 6.97 kW and then to 6.76 kW, demonstrating the bene

Journal Pre-proofs

Building upon this favorable thermal configuration, System III introduces an additional heat recovery step by capturing low-grade heat from the cooling loop to produce useful hot gas or water, which can be repurposed for tasks such as ammonia cylinder preheating or auxiliary heating. Under the ideal upper bound of $\varepsilon = 1$, System III achieves the highest efficiency of 28.33%. Importantly, because the recovered heat contribution scales with ε, System III outperforms System II for any practical case with $0 < \varepsilon < 1$, indicating a consistent benefit of additional heat integration when a usable thermal load exists.

In addition to Method 1, Method 2 is also reported to reflect the gross electrical output of the PEMFC stack under the experimental conditions where the cracker and preheater are powered externally. As shown, Method 2 yields 34.18% for System I, slightly increases to 34.95% – 35.36% for System II (Cases 1 – 3), and reaches 42.05% for System III at $\varepsilon = 1$. Therefore, Method 1 enables fair cross system comparison based on net electrical output, whereas Method 2 provides a complementary view of stack level output performance under the present experimental configuration.

Table 1 Thermal parameters and system efficiency for the three systems.

Model	NH_3 flow rate ($L \cdot min^{-1}$)	Temperature (°C)					Heat duty (kW)			System efficiency (%)	
		(1)	(2)	(3)	(4)	(5)	PH	ACr	CL	Method 1	Method 2
System I	125	25	300	700	60	—	1.03	6.97	−3.54	16.30	34.18
System II											
Case 1			250		554	60	—	7.18	−2.72	19.09	34.95
Case 2			300		518			6.97	−2.51	19.80	35.16
Case 3			350		480			6.76	−2.30	20.52	35.36
System III			300		518			6.97	−2.51	28.33	42.05

4.6 System energy density and H_2 storage capacity

This section analyzes the mass distribution, gravimetric energy density, and H_2 storage capacity of the proposed system, focusing on evaluating its scalability and mass-specific performance for aviation applications. Table S3 in Appendix A summarizes the key specifications of the experimental system as a basis for this analysis. To meet the required NH_3 feed rate of 125 $L \cdot min^{-1}$, five R-size NH_3 tanks are connected in parallel. Each tank has a volume of 57 L, with dimensions of 22.9 cm in diameter and 138 cm in height, and is filled with 22.7 kg of NH_3. This design, as validated in the above experimental session, allows a supply rate of about 25 $L \cdot min^{-1}$ of NH_3 per tank under standard operating conditions.

Fig. 9 shows the mass distribution of the current laboratory-scale system, while Fig. S11 in Appendix A illustrates the variation in the NH_3 mass fraction with increasing numbers of fuel tanks. In this analysis, only the net mass of NH_3 is considered, excluding the structural weight of the storage vessel. This simplification is reasonable, as lightweight pressure vessels, such as those made of aluminum alloys or fiber-reinforced composites, can significantly reduce storage tank weight and thereby minimize their impact on system-level mass estimation [48,49]. The six PEMFC stacks constitute 37.5% of the total mass (180 kg), while the stored NH_3, TSA purification unit, NH_3 cracker, and BOP components account for 23.6%, 23.3%, 13.1%, and 2.5%, respectively. As shown in Fig. S11, with the number of tanks increasing, the NH_3 mass fraction rises sharply and asymptotically approaches 90% of the total system mass. This trend indicates that the system has excellent energy scalability, enabling greater fuel loading, which is essential for long-endurance aviation applications.

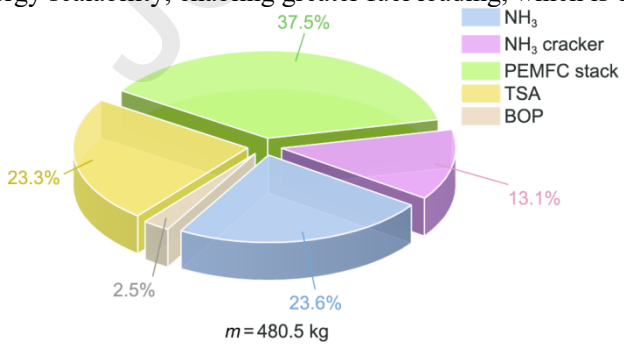

Fig. 9 Mass distribution of the NH_3-based cracking power generation system with five R-size NH_3 tanks.

Journal Pre-proofs

Fig. 10(a) presents the gravimetric energy density of the system under three configurations (Systems I – III), corresponding to energy densities are 563.0 W·h·kg^{-1} (System I), 582.5 W·h·kg^{-1} (System II), and 692.7 W·h·kg^{-1} (System III). As additional NH_3 tanks are incorporated, the total system mass increases while the available energy rises. Each system curve approaches an upper bound determined by its respective thermal efficiency, with asymptotic values reaching 2136.3 W·h·kg^{-1} for System I, 2210.0 W·h·kg^{-1} for System II, and 2628.1 W·h·kg^{-1} for System III. Notably, all three systems surpass the energy density of commercial lithium-ion batteries (~350 W·h·kg^{-1}) with as few as two NH_3 tanks, highlighting the superior weight-specific energy performance of the NH_3-PEMFC system in aviation applications.

Fig. 10(b) gives the gravimetric H_2 storage capacity of the system, defined as the mass percentage of H_2 relative to the total system mass (excluding the PEMFC stack). As the number of NH_3 tanks increases, the H_2 storage density improves and approaches the theoretical hydrogen content of pure NH_3 (17.7 wt%). With five R-size NH_3 tanks, the system achieves an H_2 storage capacity of 6.7 wt%. This behavior confirms the excellent scalability of the proposed system in terms of H_2 storage, making it well-suited for long-endurance or high-energy demand electric aviation missions.

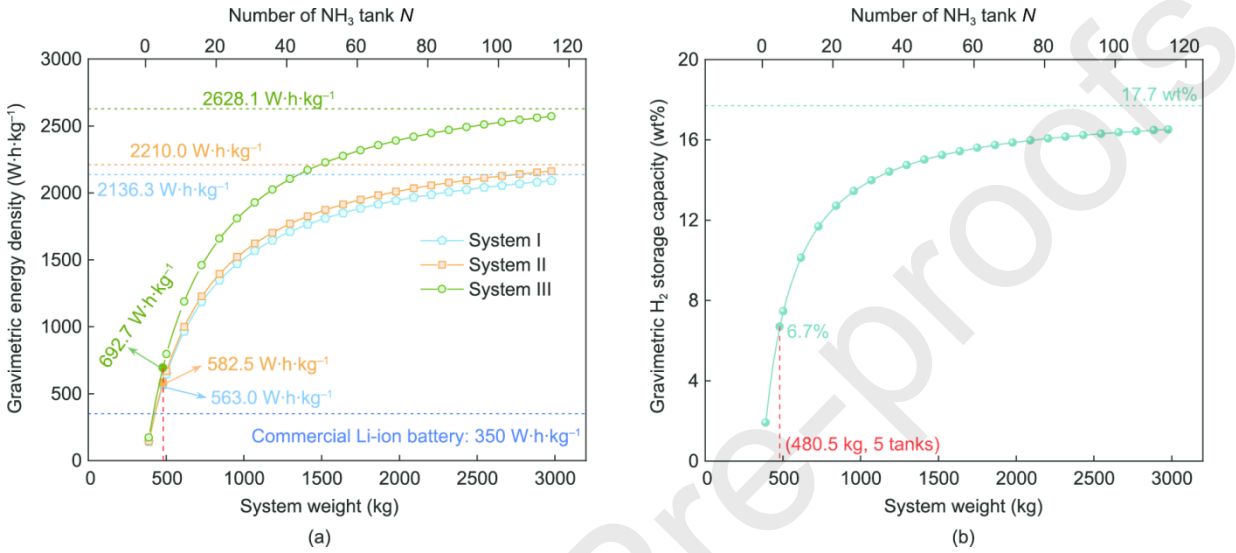

Fig. 10 Gravimetric performance evaluation of the NH_3 cracking power system under different tank configurations: (a) gravimetric energy density; (b) gravimetric H_2 storage capacity.

Moreover, we have summarized a range of representative experimental fuel-to-power generation platforms based on different hydrogen carriers and reforming technologies, as shown in Table S4. These systems reflect a diversity of design strategies and trade-offs across fuel type, H_2 production method, purification approach, power rating, and system efficiency. This overview highlights the unique characteristics and application-specific advantages of each approach. Within this broader context, compared to existing NH_3-based prototypes, which typically operate below 1 kW output, our system achieves a significantly higher rated power of 30 kW while maintaining a competitive system energy efficiency of up to 42.05%. The high and scalable gravimetric energy density of ammonia (achievable by increasing tank size or number) underscores its strong potential for aviation applications that demand both high power and excellent energy-to-weight performance.

Overall, building on the above analysis, this study presents the design, development, and evaluation of an integrated NH_3 cracking power generation system tailored for electric propulsion applications. A modular experimental prototype is constructed, delivering a maximum output power of 6 × 5 kW (30 kW), positioning it among the higher-power NH_3 fuel cell demonstrators reported to date. The system features a compact architecture, distinguishing it from traditional distributed layouts. It is explicitly designed for aviation-related applications and is also well-suited to mobile and stationary high-power energy systems. System-level simulations indicate that the compact, multifunctional reactor with integrated thermal recovery functions can significantly improve energy efficiency, confirming the effectiveness of our proposed thermal management strategy.

Despite the compact layout, the current platform still faces volume and mass constraints, owing to the use of commercially bulky furnaces for the reactor and TSA subsystems. As shown in Fig. 9, the TSA unit and NH_3 cracker together account for up to 36.4% of the total system mass, highlighting their substantial contribution to the overall weight. Future research should focus on miniaturizing these components, increasing catalyst packing density, and integrating lighter-weight heat management solutions. In particular, developing lightweight TSA units based on advanced sorbent materials or membrane-based purification could substantially reduce system mass. To further improve operational responsiveness, especially for aviation scenarios requiring rapid startup, fast-heating technologies such as induction heating or microwave-assisted cracking reactors are highly promising. Beyond component-level enhancements, the system can be advanced by integrating the ammonia cracking platform with high-temperature PEMFCs (HT-PEMFCs), solid oxide fuel cells (SOFCs), or gas turbines (GTs), enabling versatile, scalable hybrid-electric propulsion architectures for future sustainable aviation.

6. Conclusions

Journal Pre-proofs

This study presents the design of a compact and integrated NH_3 cracking power generation system for an electric propulsion system in aviation. A multi-scale validation strategy, encompassing laboratory catalyst development, engineering implementation, and system-level simulations, demonstrates the feasibility and potential of this system for aviation applications.

In catalyst development, a range of commercially available catalysts is screened, identifying a practical and scalable catalyst formulation of 1% Ru – Ni/Al_2O_3. Even in an engineering-scale reactor, a 1-meter tubular cracker packed with 340 mL of catalyst, the catalyst maintains NH_3 conversion over 99% under reaction temperatures between 600 – 700 °C and an NH_3 flow rate of 9 $L \cdot min^{-1}$, showing excellent industrial applicability. Constrained by local safety regulations, the experimental system operates at a maximum NH_3 feed rate of 23.6 $L \cdot min^{-1}$, with a TSA unit based on 13X molecular sieves, reducing residual NH_3 to the detection limit of the mass spectrometer, yielding 35.4 $L \cdot min^{-1}$ of H_2, and generating an electrical output of 2.9 kW. System simulations indicate the platform could reach 12.8 kW output at an NH_3 inlet flow rate of 125 $L \cdot min^{-1}$ while maintaining high conversion efficiency. Among the three explored thermal management strategies, the present configuration achieves a propulsion usable net electrical efficiency of 20.52%, while an optimized multi-stage heat recovery scheme increases the overall energy efficiency to 28.33% when the low-grade recovered heat is assumed fully usable. Under the experimental boundary, the gross stack output-based efficiency ranges from 34.18% to 42.05%, which is reported as a complementary metric to interpret stack level output performance and to compare operating cases within the same experimental architecture. In the practical system configuration with a 125 $L \cdot min^{-1}$ flow rate (using five R-size NH_3 tanks), the gravimetric energy density improves from 563.0 $W \cdot h \cdot kg^{-1}$ (System I) to 692.7 $W \cdot h \cdot kg^{-1}$ (System III), while the H_2 storage capacity reaches 6.7 wt%.

This research provides essential experimental evidence and theoretical guidance for NH_3-fueled electric propulsion technologies, with applicability to a broader range of electrified aviation and the related zero-carbon distributed energy applications. Future work could focus on miniaturizing the reactor and TSA unit, enhancing catalyst performance, and integrating lightweight thermal management solutions to accelerate the deployment of NH_3-based fuel cell systems toward aviation-grade specific power targets. Particular attention will also be given to aviation-specific requirements, including reducing system weight and volume, improving dynamic response under transient load conditions, and enabling rapid startup to meet mission-readiness demands.

Acknowledgments

This work was financially supported by the Innovation Technology Fund of Hong Kong (ITP/042/20AP) and Environment and Ecology Bureau of HKSAR (GTF202220122 and ECF 33/2022). The authors gratefully acknowledge the support from Automotive Parts and Accessory Systems R&D Centre (APAS).

References

[1] Sacchi R, Becattini V, Gabrielli P, Cox B, Dirnaichner A, Bauer C, et al. How to make climate-neutral aviation fly. Nat Commun 2023;14(1):3989.

[2] Wu G. A trio of commercial aircraft developments in China. Engineering 2021;7(4):424–6.

[3] Ding D, Wu XY. Evaluating the economic and carbon emission reduction potential of fuel cell electric vehicle-to-grid. DeCarbon 2025;7:100096.

[4] Aygun H. Effects of air to fuel ratio on parameters of combustor used for gas turbine engines: applications of turbojet, turbofan, turboprop and turboshaft. Energy 2024;305:132346.

[5] Jensen LL, Bonnefoy PA, Hileman JI, Fitzgerald JT. The carbon dioxide challenge facing U.S. aviation and paths to achieve net zero emissions by 2050. Prog Aerosp Sci 2023;141:100921.

[6] International Energy Agency (IEA). Aviation [Internet]. Paris: IEA; undated [cited 2026 Feb 13]. Available from: https://www.iea.org/energy-system/transport/aviation.

[7] Wheeler P, Sirimanna TS, Bozhko S, Haran KS. Electric/hybrid-electric aircraft propulsion systems. Proc IEEE 2021;109(6):1115–27.

[8] Kuśmierek A, Galiński C, Stalewski W. Review of the hybrid gas - electric aircraft propulsion systems versus alternative systems. Prog Aerosp Sci 2023;141:100925.

Journal Pre-proofs

[9] Zhou K, Zhang C, Bai H, Wang Y, Qi M, Huang L, et al. The flight verification of an integrated propulsion system powered by PEMFCs with direct airflow intake design. Appl Energy 2023;377:124432.

[10] Filippone A, Parkes B. Evaluation of commuter airplane emissions: a European case study. Transp Res Part D Transp Environ 2021;98:102979.

[11] Karthik A, Chiniwar DS, Das M, Pai MP, Prabhu P, Mulimani PA, et al. Electric propulsion for fixed wing aircrafts – a review on classifications, designs, and challenges. Eng Sci 2021;17:1–24.

[12] O'Neill S. Electric air taxis create megadeal buzz. Engineering 2022;13:5–8.

[13] Gao Y, Pan Z, Sun J, Liu Z, Wang J. High-energy batteries: beyond lithium-ion and their long road to commercialisation. Nano-Micro Lett 2022;14(1):94.

[14] Wang G, Bi Z, Zhang A, Das P, Lin H, Wu ZS. High-voltage and fast-charging lithium cobalt oxide cathodes: from key challenges and strategies to future perspectives. Engineering 2024;37:105–27.

[15] Liu Z, Peng S, Xiaokaiti P, Zhang J, You H, Abudula A, et al. Electrothermal model of all-solid-state lithium battery with composite solid-state electrolyte. EcoEnergy 2023;1(2):414–24.

[16] Peng S. Current status and future prospects of fuel cells in China. Engineering 2023;21:20–3.

[17] Du S. Recent advances in electrode design based on one-dimensional nanostructure arrays for proton exchange membrane fuel cell applications. Engineering 2021;7(1):33–49.

[18] Kendall K, Ye S, Liu Z. The hydrogen fuel cell battery: replacing the combustion engine in heavy vehicles. Engineering 2023;21:39–41.

[19] Toyota Motor Europe. New Mirai hydrogen fuel cell electric vehicle—under the skin [Internet]. Tokyo: Toyota; undated [cited 2026 Feb 13]. Available from: https://mag.toyota.co.uk/new-mirai-hydrogen-fuel-cell-electric-vehicle/.

[20] Depcik C, Cassady T, Collicott B, Burugupally SP, Li X, Alam SS, et al. Comparison of lithium ion batteries, hydrogen fueled combustion engines, and a hydrogen fuel cell in powering a small unmanned aerial vehicle. Energy Convers Manage 2020;207:112514.

[21] Qureshi F, Yusuf M, Arham Khan M, Ibrahim H, Ekeoma BC, Kamyab H, et al. A state-of-the-art review on the latest trends in hydrogen production, storage, and transportation techniques. Fuel 2023;340:127574.

[22] Wang J, Wang H, Fan Y. Techno-economic challenges of fuel cell commercialization. Engineering 2018;4(3):352–60.

[23] Usman MR. Hydrogen storage methods: review and current status. Renew Sustain Energy Rev 2022;167:112743.

[24] Asif M, Sidra Bibi S, Ahmed S, Irshad M, Shakir Hussain M, Zeb H, et al. Recent advances in green hydrogen production, storage and commercial-scale use via catalytic ammonia cracking. Chem Eng J 2023;473:145381.

[25] Jiang L, Fu X. An ammonia–hydrogen energy roadmap for carbon neutrality: opportunity and challenges in China. Engineering 2021;7(12):1688–91.

[26] Choe S, Kim N, Jang YJ. Perspective on the interfacial engineering for electrocatalytic N_2 to NH_3 conversion from catalysts to systems. EcoEnergy 2023;1(1):3–15.

Journal Pre-proofs

[27] Lin B, Nowrin FH, Rosenthal JL, Rheaume AS, Malmali M. Perspective on intensification of haber–bosch to enable ammonia production under milder conditions. ACS Sustain Chem& Eng 2023;11(27):9880–99.

[28] Solanki BS, Lim H, Yoon SJ, Ham HC, Park HS, Lee HE, et al. Recent advancement of non-noble metal catalysts for hydrogen production by NH_3 decomposition. Renew Sustain Energy Rev 2025;207:114974.

[29] Wang C, Fang J, Xu J, Ha C, Xu J, Dang C, et al. Performance evaluation and optimization for a novel supersonic precooled engine based on hydrogen production technology from ammonia cracking. Int J Hydrogen Energy 2024;52:857–71.

[30] Boretti A. Ammonia energy storage for hybrid electric aircraft. Int J Hydrogen Energy 2023;48(90):35305–15.

[31] Awad OI, Zhou B, Harrath K, Kadirgama K. Characteristics of NH_3/H_2 blend as carbon-free fuels: a review. Int J Hydrogen Energy 2023;48(96):38077–100.

[32] Park YK, Kim BS. Catalytic removal of nitrogen oxides (NO, NO_2, N_2O) from ammonia-fueled combustion exhaust: a review of applicable technologies. Chem Eng J 2023;461:141958.

[33] Lee JE, Lee J, Jeong H, Park YK, Kim BS. Catalytic ammonia decomposition to produce hydrogen: a mini-review. Chem Eng J 2023;475:146108.

[34] Xu JH, Zhang BX, Yan HZ, Ding Q, Zhu KQ, Yang YR, et al. A comprehensive assessment of the hybrid power generation system of PEMFC and internal combustion engine based on ammonia decomposition. Energy 2023;285:129559.

[35] Di Micco S, Cigolotti V, Mastropasqua L, Brouwer J, Minutillo M. Ammonia-powered ships: concept design and feasibility assessment of powertrain systems for a sustainable approach in maritime industry. Energy Convers Manage 2024;22:100539.

[36] Lin L, Zhang L, Luo Y, Luo J, Chen C, Jiang L. Highly-integrated and cost-efficient ammonia-fueled fuel cell system for efficient power generation: a comprehensive system optimization and techno-economic analysis. Energy Convers Manage 2022;251:114917.

[37] Massaro MC, Aluia F, Biga R, Accardo G, Antonio Monteverde AH. Potential of ammonia as hydrogen storage for future electrified aircraft. Energy Convers Manage 2025;X:101034.

[38] Zhang R, Liu X, Song N, He J, Cen Z, Li C, et al. Magnetic induction heating-driven rapid cold start of ammonia decomposition for hydrogen production. J Am Chem Soc 2024;146(42):28635–41.

[39] Hunter HM, Makepeace JW, Wood TJ, Mylius OS, Kibble MG, Nutter JB, et al. Demonstrating hydrogen production from ammonia using lithium imide – powering a small proton exchange membrane fuel cell. J Power Sources 2016;329:138–47.

[40] Cha J, Jo YS, Jeong H, Han J, Nam SW, Song KH, et al. Ammonia as an efficient CO_X-free hydrogen carrier: fundamentals and feasibility analyses for fuel cell applications. Appl Energy 2018;224:194–204.

[41] Zhai L, Shek Wong C, Zhang H, Xiong P, Xue X, Lun Ho Y, et al. From lab to practical: an ammonia-powered fuel cell electric golf cart system. Chem Eng J 2023;452:139390.

[42] Wang Z, Lin Y, Guo Y, Liang F, He Z, Kang L, et al. Feasibility, environmental, and economic analysis of alternative fuel distributed power systems for reliable off-grid energy supply. Appl Energy 2025;384:125493.

Journal Pre-proofs

[43] Sayas S, Morlanés N, Katikaneni SP, Harale A, Solami B, Gascon J. High-pressure ammonia decomposition on Ru–K/CaO catalysts. Catal Sci Technol 2020;10(15):5027–35.

[44] Han SJ, Bang Y, Yoo J, Seo JG, Song IK. Hydrogen production by steam reforming of ethanol over mesoporous Ni–Al_2O_3–ZrO_2 xerogel catalysts: effect of nickel content. Int J Hydrogen Energy 2013;38(20):8285–92.

[45] Hong Kong Environmental Protection Department. A guide to the chemical waste control scheme. Hong Kong: Hong Kong Environmental Protection Department; 2016.

[46] Arun M, Giddey S, Joseph P, Dhawale DS. Challenges and mitigation strategies for general failure and degradation in polymer electrolyte membrane-based fuel cells and electrolysers. J Mater Chem A Mater Energy Sustain 2025;13(16):11236–63.

[47] Okedi TI, Meyer Q, Hunter HM, Shearing PR, Brett DJ. Development of a polymer electrolyte fuel cell dead-ended anode purge strategy for use with a nitrogen-containing hydrogen gas supply. Int J Hydrogen Energy 2017;42(19):13850–9.

[48] De B, Bera M, Bhattacharjee D, Ray BC, Mukherjee S. A comprehensive review on fiber-reinforced polymer composites: raw materials to applications, recycling, and waste management. Prog Mater Sci 2024;146:101326.

[49] Chang F, Gao W, Guo J, Chen P. Emerging materials and methods toward ammonia-based energy storage and conversion. Adv Mater 2021;33(50):e2005721.

Declaration of interests

☒ The authors declare that they have no known competing financial interests or personal relationships that could have appeared to influence the work reported in this paper.

☐The authors declare the following financial interests/personal relationships which may be considered as potential competing interests:

Journal Pre-proofs